Materials Advances

ROYAL SOCIETY OF CHEMISTRY

PAPER

View Article Online
View Journal | View Issue

Cite this: *Mater. Adv.*, 2022, 3, 7590

Tuning the organelle-imaging specificity of an aggregation-induced emission luminogen with reversible mechanochromism by ionization†

Xinzhe Yang,‡[ab] Peiyu Hu,‡[c] Zeyan Zhuang,[b] Zixuan Huang,[a] Kaihang Huang,[a] Li Yin,[c] Qian Wang,*[d] Suilian Luo,[a] Guang Shi,[a] Ling Chen,*[cd] Bingjia Xu *[a] and Anjun Qin [b]

Realizing the bioimaging of different organelles usually requires organic luminophores with distinct molecular structures through a complicated chemical synthesis, which is tedious and time-consuming. Herein, an aggregation-induced emission luminogen (AIEgen) PNOy with a twisted molecular structure was prepared by employing tetraphenylethylene as the electron donor and phenylacrylonitrile-quinoline as the electron acceptor. It was found that PNOy showed a bathochromic shift of 41 nm in emission maximum under the stimulation of mechanical force. Concurrently, it could be used as a bioprobe with high specificity and biocompatibility to enable fluorescence imaging of lipid droplets (LDs) in cells. After the ionization and introduction of hexafluorophosphate as a counter ion, the resulting AIEgen PNO presented a much better stimulus-responsive performance, exhibiting a variation of 104 nm in emission maximum under the stimuli of mechanical force and acetone vapor. More impressively, PNO could be used for mitochondrial imaging with good membrane permeability and cell viability. This study demonstrates a helpful and straightforward approach to develop new bioimaging agents for different organelles and provides smart organic luminogens for innovative applications in sensing and anti-counterfeiting.

Received 7th May 2022,
Accepted 24th July 2022

DOI: 10.1039/d2ma00513a

rsc.li/materials-advances

Introduction

Organic luminescent materials have received considerable attention recently due to their promising applications in biomedical science[1–5] and information security.[6–8] Moreover, fluorescent imaging is a crucial technology for modern biology, enabling scientists to see the delicate structures of cells and monitor biological processes. However, owing to the notorious aggregation-caused quenching (ACQ) effect,[9,10] conventional organic fluorescent bioprobes with a π-conjugated system usually exhibit weak emissions in the aggregation state, which significantly limits their practical application in bioimaging. In sharp contrast, aggregation-induced emission luminogens (AIEgens) can exhibit bright emissions in the solid state or upon aggregation,[11–14] in contrast to the luminescence behaviors of conventional organic fluorescent bioprobes. Accordingly, the AIEgens can be ideal bioprobes for organelle imaging. The life activities of cells are closely related to the function of organelles. Lipid droplets (LDs) play essential roles in metabolic balance and stability, which protect the cell from lipotoxicity and lipoapoptosis.[15] Furthermore, lipid droplets contain a variety of neutral lipids and are surrounded by a single layer of phospholipids.[16,17] Since the AIE bioprobes are generally fat-soluble molecules, they may possibly enrich and dissolve in the neutral lipid of lipid droplets, which would make the lipid droplet images. On the other hand, mitochondria play vital roles in the oxidative metabolism and energy release of a cell.[18] Furthermore, the mitochondria in cancer cells have higher negative membrane potentials than those in normal cells. In this context, cationic AIEgens are highly desirable because they

[a] *School of Chemistry, Key Laboratory of Theoretical Chemistry of Environment, Ministry of Education, South China Normal University, Guangzhou 510006, China. E-mail: bingjiaxu@m.scnu.edu.cn*
[b] *State Key Laboratory of Luminescent Materials and Devices, Guangdong Provincial Key Laboratory of Luminescence from Molecular Aggregates, Center for Aggregation-Induced Emission, South China University of Technology, Guangzhou 510640, China*
[c] *State Key Lab of Respiratory Disease, Guangzhou Institutes of Biomedicine and Health, Chinese Academy of Sciences, Guangzhou 510530, China*
[d] *State Key Laboratory of Respiratory Disease, National Clinical Research Center for Respiratory Disease, Guangzhou Institute of Respiratory Health, the First Affiliated Hospital of Guangzhou Medical University, Guangzhou 510230, China. E-mail: chen_ling@gibh.ac.cn, wang_qian@gibh.ac.cn*

† Electronic supplementary information (ESI) available: Details of the synthesis, structural information for the compounds (NMR and mass spectra), Fig. S1–S14 and Table S1. See DOI: https://doi.org/10.1039/d2ma00513a

‡ These authors contributed equally to this work.

may be much easier to enrich in the mitochondria of cancer cells.[19,20]

On the other aspect, organic materials with mechanochromic properties are sensitive to the stimuli of mechanical force and solvent vapors. Therefore, they have potential applications in environmental monitors, chemical sensors, and optical data storage devices.[21–27] In general, ideal mechanochromic materials should exhibit remarkable stimulus responsiveness and reversibility.[28–31] To date, numerous AIEgens with various core structures have been developed. Although the luminescence performance of AIEgens can be improved by building strong intermolecular interactions, the strategy may not be conducive in getting significant emission wavelength variations because the stimulus-response phenomena of AIEgens in solid state usually result from the changes in intermolecular interactions.[32–35] It is worth noting that ionic AIEgens have emerged as an important class of multifunctional luminescent materials in recent years. The electrostatic repulsion of ionic AIEgens increases the distance among molecules and attenuates the intermolecular interactions, which is beneficial for altering molecular conformations and changing emission wavelengths significantly under mechanical stimuli.[36] In other words, the ionic AIEgens may be excellent candidates to produce remarkable mechanochromism. Among the AIEgens, tetraphenylethene (TPE)[37] and phenylacrylonitrile derivatives[38] have received considerable attention because of their simple molecular structures and excellent luminescent properties. Moreover, they usually have good biocompatibilities, which are favorable to bioimaging. In particular, most TPE and phenylacrylonitrile derivatives exhibit emission changes upon external stimuli.[37,38]

In this study, we present a new organic AIEgen and its ionic species, which can produce intense fluorescence to image LDs and mitochondria in cells, respectively. Herein, typical AIE moieties of TPE and phenylacrylonitrile were employed as building blocks to construct the molecule, followed by the incorporation of quinolone to offer an ionization position. As a result, a new purely organic AIEgen, namely PNOy, with a donor–acceptor (D–A) structural motif and a satisfactory fluorescence quantum yield, was achieved through this simple molecular design (Scheme 1). Since PNOy molecules are fat-soluble, they tend to accumulate in LDs. Furthermore, the highly viscous environment of the LDs restricts their intramolecular motions, thereby enabling bright fluorescence for imaging. After methylating PNOy on the nitrogen of quinolone, hexafluorophosphate was introduced as a counter anion to yield the ionic compound PNO. The methyl quinoline moiety can serve as a cationic anchor group,[39,40] making PNO available for mitochondrial imaging. In addition, both PNOy and PNO exhibit significant emission variations under mechanical force stimulation. Accordingly, these two AIEgens have the potential for sensing and bioimaging applications.

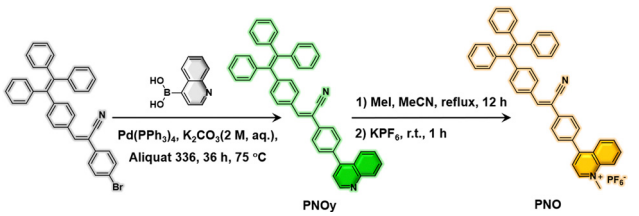

Scheme 1 Synthetic routes of the target compounds.

Results and discussion

The synthetic procedures of PNOy and PNO are outlined in Scheme 1. First, the intermediate 2-(4-bromophenyl)-3-(4-(1,2,2-triphenylvinyl)phenyl)acrylonitrile was synthesized according to the literature method, followed by the Suzuki palladium-catalyzed reaction with quinolin-4-yl boric acid to yield the product PNOy. After the methylation on the nitrogen of quinoline, an ion exchange between iodine and hexafluorophosphate was performed to obtain the target product PNO. The chemical structures of PNOy and PNO were confirmed by nuclear magnetic resonance (NMR) spectra (^{1}H NMR and ^{13}C NMR) and high-resolution mass spectra with satisfactory results (Fig. S1–S6, ESI†).

In the dilute ethyl acetate (EA) solution (Fig. S7, ESI†), PNOy showed pronounced absorption bands at around 312 nm and 368 nm, corresponding to the π–π* transition and intramolecular charge transfer (ICT) transition of the molecules, respectively. After methylation, the absorption bands of the compound were red-shifted to 321 nm and 385 nm caused by the molecular ionization and the hyperconjugation effect of the methyl group,[41] indicating the more substantial ICT effect of PNO. This inference is further supported by the variations in the photoluminescence (PL) spectra in different solvent mixtures (Fig. S8, ESI†). In particular, with the increase in solvent polarity, the PL maxima of PNOy and PNO gradually red-shifted from 527 nm and 534 nm to 550 nm and 596 nm, respectively.

Subsequently, the compounds were formulated in tetrahydrofuran (THF)/water mixtures with different contents of distilled water. In pure THF, both PNOy and PNO were weakly emissive (Fig. 1). With the increase in the water content (from 0 to 80%, v/v), there were no apparent changes in their PL spectra. However, the emission intensities of PNOy and PNO enhanced when the water content increased to 90%. Meanwhile, Mie scattering effects were observed in the UV-visible

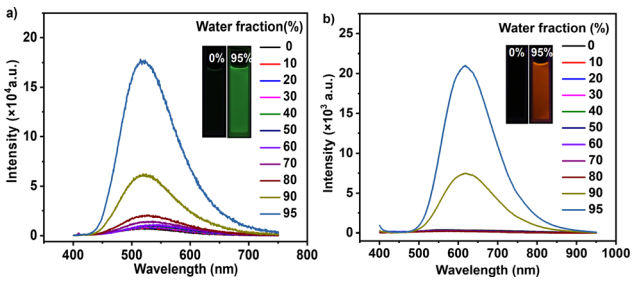

Fig. 1 AIE properties of the compounds. PL spectra of the dilute solutions of PNOy (a) and PNO (b) in water/THF mixtures with different water fractions. The insets are the emission images of PNOy in pure THF and in the water/THF mixture with 95% water fraction under the illumination of 365 nm UV light (excitation: 365 nm; concentration: 10 μM).

absorption spectra of the mixtures with high water contents (Fig. S9, ESI†), suggesting the formation of nanoaggregates. Evidently, both PNOy and PNO have AIE characteristics. When in solution, the multiple aromatic rings of the molecules rotate around the C–C bonds freely, resulting in weak luminescence. After aggregation, the molecular motions are largely restricted and the radiative decay channels are opened, leading to prominent emission enhancement.[11] In the solid state, PNOy and PNO can generate strong cyan ($\Phi_{s,o}$ = 26.3%) and orange-yellow ($\Phi_{s,o}$ = 19.1%) emissions, respectively, further demonstrating their AIE properties. The PL maxima of PNOy and PNO were separately determined to be 496 nm and 596 nm, respectively (Fig. S10, ESI†). The redder emission of PNO should be ascribed to its stronger ICT effect caused by the methylation and ionization. In addition, both PNOy (τ = 1.16 ns) and PNO (τ = 8.29 ns) gave a short lifetime in nanosecond magnitude (Fig. S11, ESI†), manifesting their fluorescence attributes in the aggregation states. The longer fluorescence lifetime and the slightly lower $\Phi_{s,o}$ value of PNO may stem from its weaker intermolecular interactions, which are likely in favor of achieving superior stimulus-responsive performance.

To gain insight into the luminescence behaviors of PNOy and PNO, theoretical calculations based on density functional theory (DFT) at the M06-2X/6-31G(d,p) level were implemented to obtain the optimized molecular structures and simulate the highest occupied molecular orbitals (HOMOs) and lowest unoccupied molecular orbitals (LUMOs) of the compounds at the ground state. As depicted in Fig. 2, the HOMO (E = −6.63 eV) of PNOy delocalized over the TPE and phenylacrylonitrile, while that of PNO (E = −7.93 eV) mainly localized on the TPE and acetonitrile moieties. Moreover, the LUMO (E = −1.49 eV) of PNOy was mainly distributed on one benzene ring of TPE, phenylacrylonitrile, and quinolone, but that of PNO (E = −5.32 eV) was located on the ionized quinoline unit. The HOMO and LUMO of PNO almost have no overlap, implying a noticeable ICT effect, which is in accordance with the experimental results. The optimized chemical structures indicate that both PNOy and PNO have a twisted molecular conformation. Accordingly, they may display emission variations under external stimuli.

As depicted in Fig. 3a, PNOy can produce a green-light emission (λ_{em} = 537 nm) upon grinding, exhibiting a moderate

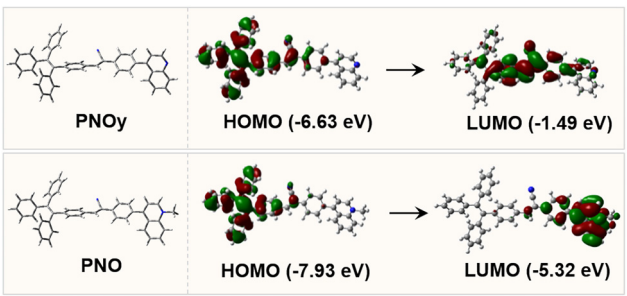

Fig. 2 The optimized molecular conformations of PNOy and PNO, as well as their HOMO and LUMO energy levels.

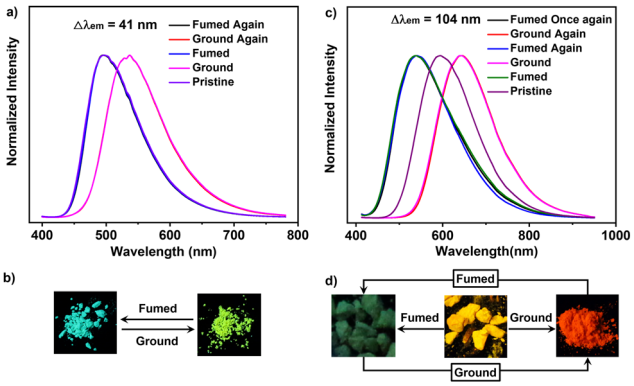

Fig. 3 (a) Emission switching of PNOy under the stimuli of mechanical force and DCM vapor. (b) The fluorescent images of the pristine and ground samples of PNOy. (c) Emission switching of PNO under the stimuli of mechanical force and acetone vapor. (d) The fluorescent images of the pristine, ground and fumed samples of PNO.

mechanochromic performance ($\Delta\lambda_{em}$ = 41 nm). Moreover, the fluorescence quantum yield of its ground sample reached 43.4%, much higher than that of the pristine one. Thus, PNOy has a force-induced emission enhancement property which is different from common AIEgens. The enhanced fluorescence intensity may be caused by the molecular planarization and the shorter intermolecular distance, leading to a higher molecular conjugation and stronger intermolecular interactions. In addition, the green fluorescence of PNOy can turn back to cyan after exposure to dichloromethane (DCM) vapor for about 20 min, suggesting that the mechanochromism of PNOy is reversible. This excellent reversibility may be associated with the strong crystallization tendency of PNOy, leading to the recovery of its molecular conformation and molecular packing mode under the stimulation of DCM vapor. In the case of PNO, its pristine sample converted into a red-light-emitting powder (λ_{em} = 643 nm) after grinding (Fig. 3b) exhibited similar mechanochromic behavior to PNOy. However, the fluorescence quantum yield of the ground sample was determined to be 10.7%, which is lower than that of the original one. Given PNO is a cationic compound, the decline of its luminescence efficiency may be associated with the repulsion among molecules, resulting in the destruction of intermolecular interactions and the increase of non-radiative channels upon grinding. Interestingly, the pristine and ground samples of PNO can transform into green-light crystals (λ_{em} = 539 nm) after exposure to acetone vapor for about 5 min.

These results suggest that the acetone vapor may induce the PNO molecules to form a new molecular packing mode and adopt a distinct molecular conformation with a weaker ICT effect. However, when the resulting crystals left the solvent atmosphere, their emission immediately red-shifted to yellow. This experimental phenomenon illustrated that the green-light crystals are meta-stable and cannot maintain their molecular packing mode without the help of acetone molecules. These variations thus implicate the possibility of PNO for acetone vapor sensing. In addition, the acetone-fumed samples of PNO

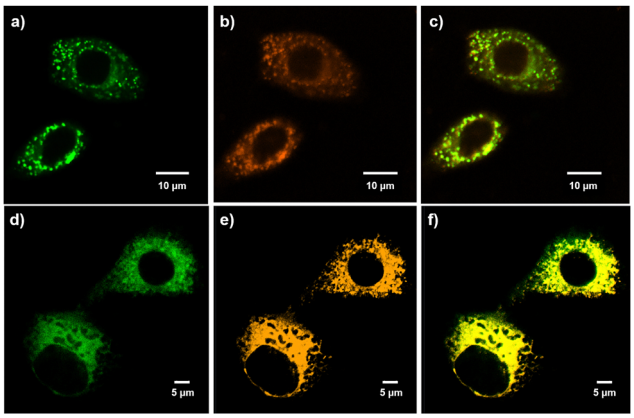

Fig. 4 CLSM images with PNOy (a–c) and PNO (d–f) in A549 cancer cells, respectively. (a) Fluorescent image of lipid droplets stained by BODIPY (green pseudocolor). (b) Fluorescent image of lipid droplets stained by PNOy (orange pseudocolor). (c) An overlay image of parts (a) and (b). (d) Fluorescent image of mitochondria stained by MitoTracker Green (green pseudocolor). (e) Fluorescent image of mitochondria stained by PNO (orange pseudocolor). (f) An overlay image of parts (d) and (e) (excitation: 405 nm; concentration: 10 μM).

can also turn into a red-light powder by grinding. Given this, the fluorescence of PNO is switchable between green and red under mechanical force and acetone vapor stimuli, showing a remarkable emission variation up to 104 nm.

Notably, both the pristine and ground samples of PNOy showed sharp diffraction peaks in the X-ray diffraction (XRD) patterns (Fig. S12, ESI†). Moreover, their differential scanning calorimetry (DSC) thermograms also presented an intense endothermic peak at around 208 °C (Fig. S13, ESI†). These experimental results elaborate that PNOy has high crystallinity and its molecules build robust intermolecular interactions in the crystalline state, which are not easily destroyed by grinding. As a result, PNOy only presented a moderate mechanochromism performance. By contrast, the pristine sample and the fumed sample in the air of PNO exhibit relatively low crystallinities, as indicated by the less and weak diffraction peaks in the XRD patterns. Moreover, their melting points in the DSC thermograms (161 °C for the pristine sample and 145 °C for the fumed sample) are much lower than those of PNOy. These data demonstrate that the PNO molecules can only build weak interactions in the aggregation states. Therefore, the molecular conformations of PNO can be easily changed by external stimuli, resulting in evident emission alterations.

As motivated by the satisfactory AIE performance of PNOy and PNO, bioimaging was then conducted for cancer cells. It is worth noting that biocompatibility is an essential parameter for biological analysis and clinical diagnosis. Consequently, CCK8 counting kits were used to evaluate the cytotoxicity of PNOy and PNO. The studies on dose-dependent cytotoxicity illustrated that the A549 cancer cells still exhibited high survival when the concentrations of PNOy and PNO reached 20 μM (Fig. S14, ESI†). Thus, the good biocompatibilities to the cells make these two AIEgens suitable candidates for bioimaging.

Subsequently, A549 cells were incubated with 10 μM of either PNOy or PNO for 2 h. We surveyed the cell behaviors by confocal laser scanning microscopy (CLSM), and the results showed that both PNOy and PNO could penetrate the cell membranes and enter the organelles. Subsequently, a commercial staining agent, BODIPY, was used for colocalization experiments to evaluate the LD imaging performance. It was found that PNOy could selectively concentrate in LDs and emit strong green fluorescence (λ_{em} = 501 nm) to image these organelles (Fig. 4a–c). The Pearson's coefficient between PNOy and BODIPY was calculated to be 0.87, suggesting that PNOy is a promising candidate for LD imaging. By contrast, PNO could specifically anchor the mitochondria and then produce intense orange-yellow fluorescence (λ_{em} = 598 nm) to visualize these energy generators in the cells. Fig. 4d–f illustrate that PNO highly overlap with MitoTracker Green, and the corresponding Pearson's coefficient was determined to be 0.84. Accordingly, it may serve as a new staining agent for mitochondrial imaging. These results fully demonstrate that PNOy and PNO from the same AIE system can selectively and efficiently image different organelles. Their satisfactory fluorescence quantum yields and Pearson's coefficients are comparable to most typical AIEgens that are used for LD and mitochondrion imaging.[42,43] Consequently, the ionization of AIEgens may be a helpful and straightforward approach for developing excellent staining agents for distinct organelles.

Conclusions

In summary, a twisted organic luminophore PNOy and its corresponding ionic compound PNO were prepared and found to show prominent AIE properties. They presented high fluorescence quantum yields of 26.3% and 19.1%, respectively, in the solid-state. Furthermore, PNOy exhibited reversible mechanochromism with an emission alteration of 41 nm. For PNO, its fluorescence can be switched between green and red by mechanical force and acetone vapor stimuli, showing a remarkable emission variation up to 104 nm. Furthermore, PNOy and PNO can concentrate in LDs and mitochondria, respectively, and produce intense fluorescence to selectively image the organelles in cells. These results demonstrate that PNOy and PNO are multifunctional AIEgens that are promising for sensing, anti-counterfeiting, and bioimaging applications.

Author contributions

B. Xu, Q. Wang, and L. Chen designed the experiments. X. Yang, P. Hu, Z. Zhuang, Z. Huang, K. Huang, L. Yin, and Q. Wang performed the experiments. B. Xu, X. Yang, and Z. Zhuang wrote the manuscript. All the authors were involved in the analysis and interpretation of data.

Conflicts of interest

There are no conflicts to declare.

Acknowledgements

This work was supported by the National Natural Science Foundation of China (51603233), the Natural Science Foundation of Guangdong Province of China (2019A1515010550), and the Guangzhou Municipal Science and Technology Project (201904010435).

Notes and references

1 C. Ji, L. Lai, P. Li, Z. Wu, W. Chen and M. Yin, *Aggregate*, 2021, **2**, e39.
2 M. Jiang, R. T. K. Kwok, X. Li, C. Gui, J. W. Y. Lam, J. Qu and B. Z. Tang, *J. Mater. Chem. B*, 2018, **6**, 2557–2565.
3 D. Wang, H. Su, R. T. K. Kwok, G. Shan, A. C. S. Leung, M. M. S. Lee, H. H. Y. Sung, I. D. Williams, J. W. Y. Lam and B. Z. Tang, *Adv. Funct. Mater.*, 2017, **27**, 1704039.
4 S. Liu, H. Ou, Y. Li, H. Zhang, J. Liu, X. Lu, R. T. K. Kwok, J. W. Y. Lam, D. Ding and B. Z. Tang, *J. Am. Chem. Soc.*, 2020, **142**, 15146–15156.
5 W. Cheng, H. Chen, C. Liu, C. Ji, G. Ma and M. Yin, *View*, 2020, **1**, 20200055.
6 Z. Chi, X. Zhang, B. Xu, X. Zhou, C. Ma, Y. Zhang, S. Liu and J. Xu, *Chem. Soc. Rev.*, 2012, **10**, 3878–3896.
7 B. Xu, H. Wu, J. Chen, Z. Yang, Z. Yang, Y. Wu, Y. Zhang, C. Jin, P. Lu, Z. Chi, S. Liu, J. Xu and M. Aldred, *Chem. Sci.*, 2017, **8**, 1909–1914.
8 Y. He, S. Lin, J. Guo and Q. Li, *Aggregate*, 2021, **2**, e141.
9 Z. Zhelev, H. Ohba and R. Bakalova, *J. Am. Chem. Soc.*, 2006, **128**, 6324–6325.
10 H. N. Kim, M. H. Lee, H. J. Kim, J. S. Kim and J. Yoon, *Chem. Soc. Rev.*, 2008, **37**, 1465–1472.
11 J. Luo, Z. Xie, J. W. Y. Lam, L. Cheng, H. Chen, C. Qiu, H. S. Kwok, X. Zhan, Y. Liu, D. Zhu and B. Z. Tang, *Chem. Commun.*, 2001, 1740–1741.
12 R. T. K. Kwok, C. W. T. Leung, J. W. Y. Lam and B. Z. Tang, *Chem. Soc. Rev.*, 2015, **44**, 4228–4238.
13 R. Crespo-Otero, Q. Li and L. Blancafort, *Chem. – Asian J.*, 2019, **14**, 700–714.
14 Y. Chen, J. W. Y. Lam, R. T. K. Kwok, B. Liu and B. Z. Tang, *Mater. Horiz.*, 2019, **6**, 428–433.
15 Z. Wang, C. Gui, E. Zhao, J. Wang, X. Li, A. Qin, Z. Zhao, Z. Yu and B. Z. Tang, *ACS Appl. Mater. Interfaces*, 2016, **8**, 10193–10200.
16 T. C. Walther and R. V. F. Jr., *Biochim. Biophys. Acta*, 2009, **1791**, 459–466.
17 M. Beckman, *Science*, 2006, **311**, 1232–1234.
18 S. Anoopkumar-Dukie, T. Conere, G. D. Sisk and A. Allshire, *Br. J. Radiol.*, 2009, **82**, 847–854.
19 C. Y. Y. Yu, H. Xu, S. Ji, R. T. K. Kwok, J. W. Y. Lam, X. Li, S. Krishnan, D. Ding and B. Z. Tang, *Adv. Mater.*, 2017, **29**, 1606167.
20 G. Feng, W. Qin, Q. Hu, B. Z. Tang and B. Liu, *Adv. Healthcare Mater.*, 2015, **4**, 2667–2676.
21 D. Ding, K. Li, B. Liu and B. Z. Tang, *Acc. Chem. Res.*, 2013, **46**, 2441–2453.
22 S. Chen, Y. Hong, Y. Liu, J. Liu, C. W. T. Leung, M. Li, R. T. K. Kwok, E. Zhao, J. W. Y. Lam, Y. Yu and B. Z. Tang, *J. Am. Chem. Soc.*, 2013, **135**, 4926–4929.
23 M. Jiang, X. Gu, R. T. K. Kwok, Y. Li, H. H. Y. Sung, X. Zheng, Y. Zhang, J. W. Y. Lam, I. D. Williams, X. Huang, K. S. Wong and B. Z. Tang, *Adv. Funct. Mater.*, 2018, **28**, 1704589.
24 X. Gu, E. Zhao, T. Zhao, M. Kang, C. Gui, J. W. Y. Lam, S. Du, M. M. T. Loy and B. Z. Tang, *Adv. Mater.*, 2016, **28**, 5064–5071.
25 J. Qian and B. Z. Tang, *Chem*, 2017, **3**, 56–91.
26 J. Mei, Y. Huang and H. Tian, *ACS Appl. Mater. Interfaces*, 2018, **10**, 12217–12261.
27 X. Cai, F. Hu, G. Feng, R. T. K. Kwok, B. Liu and B. Z. Tang, *Isr. J. Chem.*, 2018, **58**, 860–873.
28 S. Yoon, J. W. Chung, J. Gierschner, K. S. Kim, G. Choi, D. Kim and S. Y. Park, *J. Am. Chem. Soc.*, 2010, **132**, 13675–13683.
29 X. Luo, J. Li, C. Li, L. Heng, Y. Q. Dong, Z. Liu, Z. Bo and B. Z. Tang, *Adv. Mater.*, 2011, **23**, 3261–3265.
30 W. Yuan, Y. Tan, Y. Gong, P. Lu, J. W. Y. Lam, X. Y. Shen, C. Feng, H. H.-Y. Sung, Y. Lu, I. D. Williams, J. Z. Sun, Y. Zhang and B. Z. Tang, *Adv. Mater.*, 2013, **25**, 2837–2843.
31 W. Qiao, P. Yao, Y. Chen, Q. Xiao, L. Zhang and Z. Li, *Mater. Chem. Front.*, 2020, **4**, 2688–2696.
32 Y. Gong, G. Chen, Q. Peng, W. Z. Yuan, Y. Xie, S. Li, Y. Zhang and B. Z. Tang, *Adv. Mater.*, 2015, **27**, 6195–6201.
33 Y. Chen, C. Xu, B. Xu, Z. Mao, J. Li, Z. Yang, N. R. Peethani, C. Liu, G. Shi, F. L. Gu, Y. Zhang and Z. Chi, *Mater. Chem. Front.*, 2019, **3**, 1800–1806.
34 M. Tanioka, S. Kamino, A. Muranaka, Y. Ooyama, H. Ota, Y. Shirasaki, J. Horigome, M. Ueda, M. Uchiyama, D. Sawada and S. Enomoto, *J. Am. Chem. Soc.*, 2015, **137**, 6436–6439.
35 J. Yang, J. Qin, P. Geng, J. Wang, M. Fang and Z. Li, *Angew. Chem., Int. Ed.*, 2018, **57**, 14174–14178.
36 X. Yang, Q. Wang, P. Hu, C. Xu, W. Guo, Z. Wang, Z. Mao, Z. Yang, C. Liu, G. Shi, L. Chen, B. Xu and Z. Chi, *Mater. Chem. Front.*, 2020, **43**, 941–949.
37 Z. Yang, Z. Chi, Z. Mao, Y. Zhang, S. Liu, J. Zhao, M. P. Aldred and Z. Chi, *Mater. Chem. Front.*, 2018, **2**, 861–890.
38 Z. Chi, X. Zhang, B. Xu, X. Zhou, C. Ma, Y. Zhang, S. Liu and J. Xu, *Chem. Soc. Rev.*, 2012, **10**, 3878–3896.
39 X. Yang, N. Wang, L. Zhang, L. Dai, H. Shao and X. Jiang, *Nanoscale*, 2017, **9**, 4770.
40 Y. Li, J. Zhuang, Y. Lu, N. Li, M. Gu, J. Xia, N. Zhao and B. Z. Tang, *ACS Nano*, 2021, **15**, 20453–20465.
41 N. Zhao, Z. Yang, J. W. Y. Lam, H. H. Y. Sung, N. Xie, S. Chen, H. Su, M. Gao, I. D. Williams, K. S. Wong and B. Z. Tang, *Chem. Commun.*, 2012, **48**, 8637–8639.
42 L. Wang, X. Chen, X. Ran, H. Tang and D. Cao, *Dyes Pigm.*, 2022, **203**, 110332.
43 K. Yu, J. Pan, E. Husamelden, H. Zhang, Q. He, Y. Wei and M. Tian, *Chem. – Asian J.*, 2020, **15**, 3942–3960.